Research Article

TRR
JOURNAL OF THE TRANSPORTATION RESEARCH BOARD

Transportation Research Record
2022, Vol. 2676(6) 217–235

DOI: 10.1177/03611981221074366
journals.sagepub.com/home/trr
SAGE

Real-Time Arterial-Friendly Ramp Metering System

Yao Cheng[1], Yen-Yu Chen[2], and Gang-Len Chang[1]

Abstract

To balance the benefits between the freeway and arterial users and also to prevent on-ramp queue spillbacks, the authors have developed an arterial-friendly local ramp metering control (AF-ramp) system for time-of-day operations during recurrent congestion. This study presents the real-time version of the AF-ramp (named RAF-ramp) system, with a lane-group-based macroscopic traffic module for predicting traffic state and for executing control strategies, aiming at maximizing the total throughput from the control area, comprising the ramp meter and nearby local intersection signals. Recognizing the discrepancy in the dynamic nature between ramp traffic and arterial flows, the RAF-ramp system with its embedded traffic state prediction and monitoring mechanism can trigger the concurrent optimization of both controls when justified to do so, or only dynamically adjust the ramp metering rate under the pre-optimized local signal environment. The results of extensive simulation experiments have confirmed that the proposed system outperforms the widely-applied real-time ramp control model, ALINEA/Q, under various experimental traffic scenarios, because the produced control strategies can effectively utilize the freeway's weaving capacity and also best coordinate neighboring intersections' signals to maximize the entire network's performance. Such a real-time arterial-friendly ramp metering system, addressing both the time-varying freeway dynamics and the concerns of local traffic users, may well serve as an effective tool for contending with bottlenecks at freeway interchanges.

Keywords

operations, freeway operations, active traffic management, freeway traffic control, ramp metering

Ramp metering has been viewed by the traffic community as an effective strategy to contend with local freeway bottlenecks caused by ramp merging flows. The green-red signal located at an on-ramp is implemented to regulate and break up the on-ramp vehicle platoons. However, by doing so, it often incurs excessive ramp vehicle delays and overflows to the local arterials during high on-ramp demand periods. Although one may cope with such issues by either increasing the metering rate or suspending ramp control, those tactics will inevitably render the ramp metering control less effective in mitigating the freeway's congestion.

To balance the benefits (or costs) between the freeway and arterial users in contending with recurrent interchange congestion, Cheng and Chang (*1*) have developed an arterial-friendly local ramp metering control system for time-of-day and off-line operations. This study is to enhance their off-line system with a lane-group-based macroscopic traffic prediction module for real-time operations at freeway interchanges experiencing highly fluctuating traffic demands.

From reviewing the literature, most existing models on local ramp control are operated in either fixed-time or traffic-responsive mode, depending on the availability of real-time traffic information. First put into practice in Chicago, IL in 1963 (*2*), the fixed-time ramp metering control has since been deployed in several metropolitan areas (Los Angeles, CA, 1968; Minneapolis-St. Paul, MN, 1970; Seattle, WA, 1981; Denver, CO, 1981; Portland, OR, 1981; Detroit, MI, 1984). However, the

[1]Department of Civil & Environmental Engineering, University of Maryland, College Park, MD
[2]Department of Transportation & Logistics Management, National Yang Ming Chiao Tung University, Hsinchu City, Taiwan

Corresponding Author:
Yen-Yu Chen, yychen804@gmail.com

core logic of such control with pre-determined metering rates on a time-of-day basis often fails to achieve the desired level of performance when traffic volumes significantly deviate from the historical patterns. Recognizing such deficiencies, several researchers have proposed various traffic-responsive local metering control strategies (*3–9*) to contend with the time-varying traffic volume. Among them, ALINEA (*4*, *5*), a local feedback control ramp metering control strategy, is the most widely referenced. The ramp metering rates under such control are determined based on the difference between the observed occupancies downstream of the on-ramp segment and a preset critical value calibrated from historical data. Recognizing the limitation of local ramp metering strategies for congestion patterns spreading over multiple ramps, traffic researchers have further developed various coordinated ramp metering strategies for system-wide congestion controls (*10–18*).

For all the aforementioned strategies, despite their reported effectiveness in mitigating freeway congestion, their field deployment often faces resistance from local traffic agencies and nearby arterial users. This is because such strategies with the control objective of improving traffic conditions on the freeway often incur excessive ramp vehicle queues and spillback to block local traffic (*19*, *20*). Noticeably, the concerns of ramp overflows in practice have mostly been addressed by restricting the metering rates with so-called queue override functions (*7*, *10*, *12*, *21*, *22*). However, given that most locations where it would be justified to implement ramp metering control are likely to experience high freeway and on-ramp volumes, those queue override functions may be frequently triggered by the detectors, thus significantly degrading the effectiveness of metering controls.

To address such negative impacts on local traffic, some limited studies in the literature further included local intersections near the on-ramp in the control area so that nearby traffic signals can better coordinate with the ramp metering control (*23–26*). Nevertheless, such control systems continue to place the freeway's performance as their primary control objective with insufficient attention to the concerns often raised by local traffic users. To balance the benefits between the freeway and arterial users within a congested on-ramp area, Cheng and Chang (*1*) have designed an arterial-friendly local ramp metering (named AF-ramp) control strategy to concurrently optimize the ramp metering rate and signal plans at those intersections feeding traffic to a freeway's on-ramp under time-of-day or off-line operations.

As a natural extension for the off-line AF-ramp model, this study proposes a real-time arterial-friendly ramp metering (RAF-ramp) system which aims to maximize the total throughput and concurrently prevent on-ramp spillovers with optimized signal controls at nearby intersections. More specifically, the RAF-ramp can effectively prevent not only on-ramp queues from spilling back to local intersections but also spillovers on arterial links by excessive traffic volumes turning onto the ramps during peak periods. Recognizing the discrepancy in the dynamic nature between ramp metering and signal controls, the RAF-ramp system, embodied with a traffic state monitoring mechanism, can trigger the concurrent optimization of both controls when justified to do so. Otherwise, the system will let the ramp dynamically adjust its metering rate under the optimized local signal control environment. Such a real-time arterial-friendly system, addressing both the time-varying traffic dynamics and the concerns of local traffic users, may well serve as an effective strategy to contend with the bottleneck at freeway interchanges. The key system features of the proposed RAF-ramp system include:

- respond to time-varying traffic volumes on both the freeway and its neighboring arterial in a timely manner with proactive ramp and signal controls, based on the embedded lane-group-based traffic predicting module;
- embody a traffic state monitoring mechanism to govern the optimal timings for implementing either the dynamic metering cycles alone or a system-wide update to concurrently reoptimize signal plans for all nearby intersections;
- maximize the total throughput for both the freeway and arterial links within the control area based on the real-time detected flows;
- prevent ramp queues from spilling back to neighboring streets by coordinating their signal plans with ramp metering control;
- optimize the signal plan, including the cycle length, green splits, and phase sequences, for each nearby intersection to ensure that the traffic flows heading toward the on-ramp will not cause turning bay spillover; and
- provide local progression for all path flows within the control area of the local arterial with a set of optimal offsets to avoid the local arterial's bottlenecks.

RAF-Ramp System

Figure 1 shows the operational flowchart of the proposed RAF-ramp system and its principal components, where the entire control process consists of the following three main stages: (i) system initialization and assessment, (ii) projection of traffic evolution pattern and selection of the initial ramp metering cycle, and (iii) dynamic execution of the integrated ramp and local signal controls,

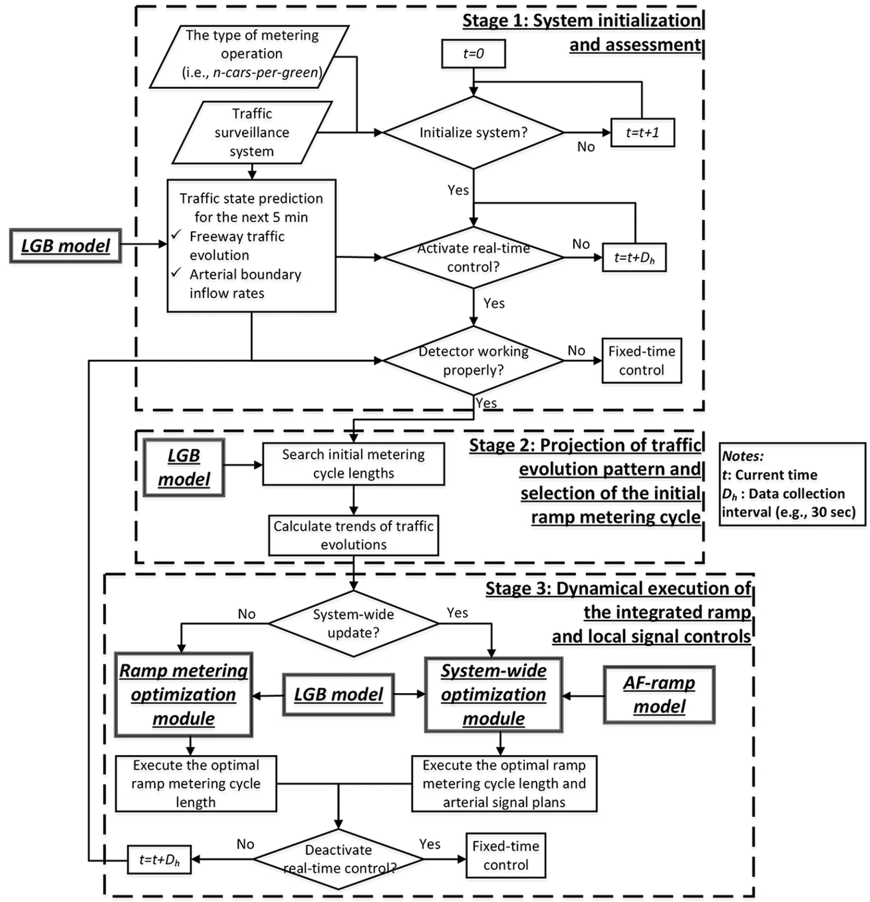

Figure 1. Operational flowchart of the proposed real-time arterial-friendly ramp (RAF-ramp) system.

based on predicted traffic conditions with the embedded lane-group-based (LGB) model (*26*) and the system-wide optimization module for the concurrent update of ramp metering cycle and neighboring signal plans.

The control boundaries for such a system and the locations of vehicle detectors for real-time traffic monitoring and performance assessment are shown in Figure 2. A brief description of key activities at each control stage is presented below:

Stage 1: Initialization and Assessment

At this stage, the proposed system shall first perform its real-time monitoring of the target area's traffic conditions, and then determine when to activate the real-time operations. An essential task to be done concurrently with traffic monitoring is to constantly assess the detectors' data quality and reliability. Some well-established methods for such needs can be found in the literature (*27*, *28*). The core concepts for system initialization and traffic state monitoring are reported below:

System Initialization. Since the LGB module needs the initial roadway traffic conditions from sensor data to project the traffic state evolution over the selected future time horizon, one can select the time period of 30 to 60 min before the peak hours for system initialization, mainly to ensure that its interactions with traffic detectors work as expected and the projected traffic states are consistent with observed conditions.

Traffic State Monitoring and Prediction. At each current time interval t, the system shall employ the LGB model to predict the flow rates on the freeway segment upstream of the on-ramp over the next N time intervals (i.e., $t + 1$ to $t + N$), denoted as $W_t(t + n)$, where $n = 1, \ldots, N$. Therefore, the expected flow rate on the freeway segment upstream of the on-ramp for a projected time interval k, denoted as $\hat{W}(k)$, can be calculated with the average of all flow rates predicted from all preceding (k-N) intervals to the current interval t. The mathematical expression of such a process is shown below:

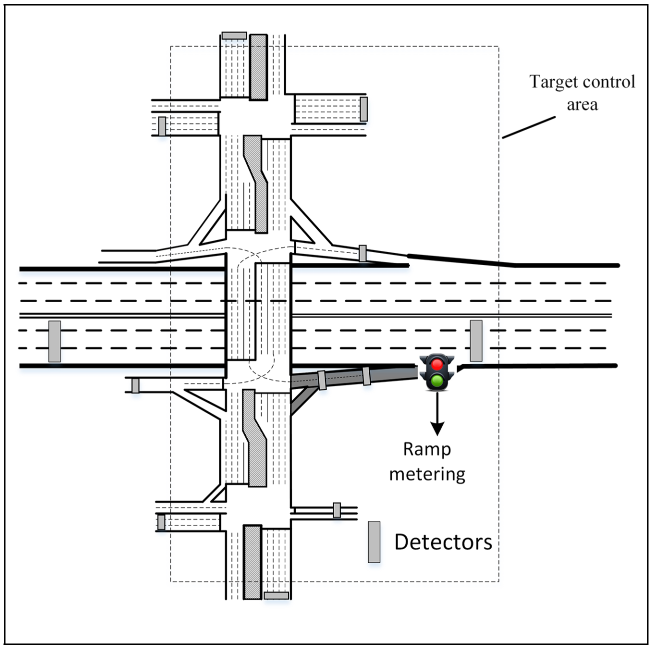

Figure 2. Detector locations and the target control area for deploying the real-time arterial-friendly ramp (RAF-ramp) system.

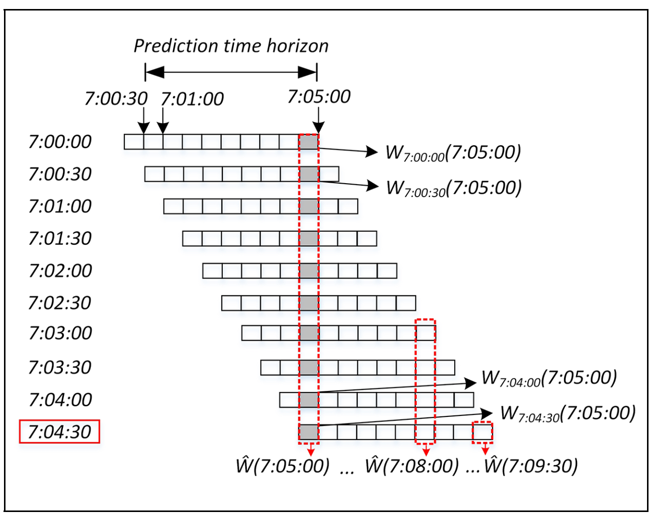

Figure 3. Example of computing the expected flow rate for the projected time interval.

$$\hat{W}(k) = \frac{W_{k-N}(k) + W_{k-N+1}(k) + \ldots + W_t(k)}{N-(k-t)+1} \tag{1}$$

For example, as shown in Figure 3, given that the duration of each time interval is 30 s and with N equal to 10 at the current time of 7:00:00 a.m., the system will produce the projected traffic states up to 7:05:00 a.m. at the time unit of every 30 s. Keeping the same prediction exercise, the system with the LGB model up to 7:04:30 a.m. will have 10 predicted traffic flow rates for the interval of 7:05:00 a.m., that is, $W_{7:00:00}(7{:}05{:}00)$, $W_{7:00:30}(7{:}05{:}00)$, …, $W_{7:04:30}(7{:}05{:}00)$. Then, the system will take the average of those 10 predicted results as the expected flow rate for the 7:05:00 a.m. interval (i.e., $\hat{W}(7:05:00)$). Following the same logic, one can compute the expected flow rates for the following nine time intervals (i.e., 7:05:30 to 7:09:30 a.m.).

Given a series of predicted flow rates over the projected time horizon, one can then calibrate the trend for the flow rates, using all obtained $\hat{W}(k)$, where $k = t + 1$ *to* $t + N$, and the slope, a_1, indicates the evolution trend of $\hat{W}(k)$ over the projected N intervals.

$$f(k) = a_1 \cdot k + b_1 \tag{2}$$

Table 1. Assessment Process for Activating the Real-Time Control

Step 1
At time *t*,
If (at least half of $\hat{W}(k)$ in the next 5 min $> \gamma_1$) **and** ($a_1 \geqslant 0$)
then go to Step 3;
else go to Step 2;
Step 2
If (at least half of the detected flow rates on the freeway segment upstream of the on-ramp over the past 5 min $> \gamma_2$)
then go to Step 3;
else go to Step 4;
Step 3
Stop **and** activate real-time control;
Step 4
$t=t + D_h$ **and** go to step 1.

Note: a_1 = slope of the trend line of $\hat{W}(k)$ in the next 5 min; D_h = data collection interval (e.g., 30 s).

Activation Mechanism. After initialization, this system will then assess the necessity of activating the real-time control based on the predicted and detected traffic states on the freeway segments upstream of the on-ramp. The main concept is that if half or more of those predicted (detected) flow rates in the subsequent (past) 5 min exceed the preset thresholds, then the real-time control ought to be activated. The assessment algorithm is detailed in Table 1.

Stage 2: Projection of Traffic Evolution Patterns and Selection of the Initial Ramp Metering Cycle

The primary task at Stage 2 is to search the best initial cycle length for ramp metering for the next system-wide control, given the freeway's flow rates and the arterial's signal plans at the current time interval t. More specifically, the system will first employ its LGB model to predict the freeway's throughputs for each time interval over the next 5 min, and then apply a search algorithm to identify the corresponding metering cycle that can

Table 2. Operational Process for the Search of the Optimal Initial Cycle Length for Ramp Metering Control

At the current time t,
Step 1
Set $t_a = t$ **and** metering cycle length (C_0) $= C_{o,min}$
Step 2
Predict freeway throughput ($V^F_{t_a,C_o}$) of the period (t_a) to ($t_a + D_h$) with a given metering cycle length, C_o, with the LGB model.
Step 3
If $C_o < C_{o,max}$
then $C_o = C_o + 1$ **and** go to Step 2.
else go to Step 4.
Step 4
Choose the metering cycle length with maximal freeway throughput as the preliminary optimal cycle length ($\hat{C}_{ta}$) for the period (t_a) to ($t_a + D_h$).
Step 5
If $(t_a - t) < 300\,s$
then set $t_a = t_a + D_h$ **and** $C_o = C_{o,min}$ **and** go to Step 2
else stop **and** output the optimal metering cycle lengths

Note: $C_{o,min}$ = prespecified lower bound of the metering cycle length; $C_{o,max}$ = prespecified upper bound of the metering cycle length; and D_h = data collection frequency (i.e., 30 s).

achieve the maximal freeway throughput if the discrepancies between projected and actual traffic conditions are within the acceptable range. Such a metering cycle will be subjected to revision after every 30 s, using the local metering algorithm reported later in Stage 3. The step-by-step description of the control process and search algorithm at this stage is shown in Table 2.

Primary information produced from this stage of operations per 5 min includes: (i) the predicted flow rates on the freeway segment upstream of the on-ramp; (ii) the predicted arterial boundary inflow rates; (iii) the differences between the detected and predicted inflow rates over the arterial's control boundaries; and (iv) the detected occupancies at the on-ramp and their evolution patterns.

Stage 3: Dynamical Execution of the Integrated Ramp and Local Signal Controls

System-Wide Update Mechanism. With the information from previous stages, at this stage, as shown in Figure 4, the RAF-ramp system will determine if a system-wide update (i.e., concurrently update the ramp metering cycle length and arterial signal plans) is needed or stay with the dynamic ramp control only for the next interval of 5 min.

The core logic for Stage 3 assessment is first to estimate the on-ramp queues under the initial metering cycle produced at Stage 2 and project the arterial flow rates moving into the control area, and then evaluate the need for the system-wide update under the following conditions:

- The initial ramp metering cycle lengths from Stage 2 will cause the on-ramp queue to spill back in the next 5 min, based on the assessment process shown in Step 1 in Table 3, where $\Theta(Q^A)$ is the prespecified maximum allowable ramp metering cycle under the critical arterial traffic volume, Q^A, that can ensure no overflows at the ramp over the next 5 min.
- The on-ramp is currently experiencing queue overflows, based on the occupancies detected by the on-ramp detectors (see Step 2 in Table 3).
- The on-ramp queues are projected to consistently decrease over the next 5 min, based on the estimation process shown in Step 3 of Table 3.

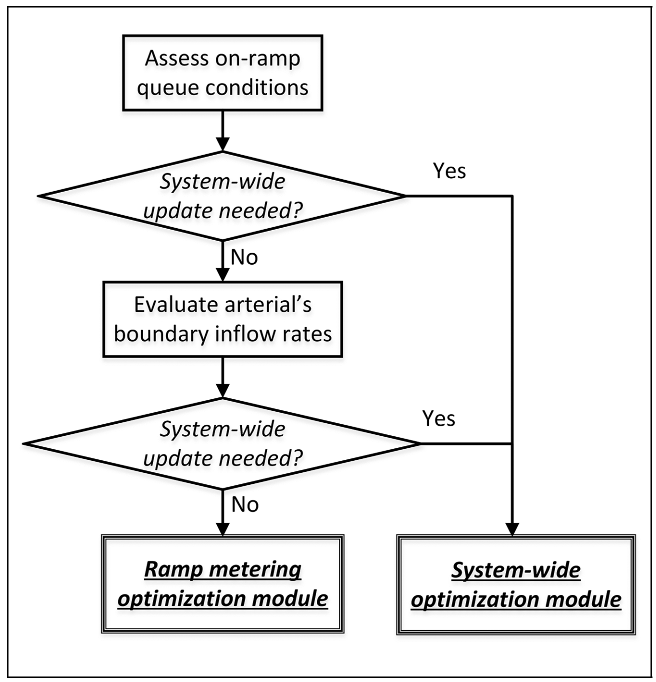

Figure 4. Flowchart of the system-wide update mechanism.

Note that if the differences between the predicted and detected arterial inflow rates to the control area over the

Table 3. Procedure for Assessing the On-Ramp's Queue Conditions

Step 1
If (at least half of the initial metering cycles for ramp control over the next 5 min determined in Stage 2 $> \Theta(Q^A)$) **and** (S(predicted flow rates on the freeway segment upstream of the on-ramp) ≥ 0) **and** (S(predicted local boundary inflow rates) ≥ 0)
then go to Step 4;
else go to Step 2;
Step 2
If (S(predicted arterial boundary inflow rates) ≥ 0) **and** (S(detected occupancy rates of the upstream detector of the on-ramp) ≥ 0) **and** ($\sigma_u^O(t - n_1 \cdot D_h) \geq 25\%,\ n_1 = 0$ *and* 1) **and** ($\sigma_m^O(t - n_2 \cdot D_h) \geq 25\%,\ n_2 = 0,\ 1,\ \ldots,\ 5$)
then go to Step 4;
else go to Step 3;
Step 3
If (S(detected occupancy rates at the middle detector on the on-ramp) < 0) **and** (S(predicted arterial boundary inflow rate) ≤ 0)
then go to Step 4;
else go to Step 5;
Step 4
Stop **and** output **"**system-wide update needed.**"**
Step 5
Stop **and** output **"**system-wide update not needed.**"**

Note: $\sigma_u^O(t)$ and $\sigma_m^O(t)$ = the occupancy rates of the upstream and middle detectors on the on-ramp at time t, respectively; D_h = data collection frequency (e.g., 30 s).
An occupancy threshold of 25% is used to determine whether the queue has reached the vehicle detectors or not (29).

Table 4. Procedure for Deactivation of Real-Time Control

Step 1
At time t, for the past 10 min,
If (the computed ramp metering cycle lengths = $C_{o,\,min}$) **and** ($\sigma_u^O(k') < \gamma_5$) **and** (detected arterial boundary inflow rates $< \gamma_6$) **and** (S(detected arterial boundary inflow rates) ≤ 0)
then go to Step 2;
else go to Step 3;
Step 2
Stop **and** deactivate real-time control
Step 3
Stop **and** continue real-time control

Note: $C_{o,\,min}$ = a prespecified lower bound of the metering cycle length; $\sigma_u^O(k')$ = occupancy rates of the upstream detectors on the on-ramp at time k'; $S(.)$ = the slope of the trend line of the target variable; γ_5 and γ_6 = predefined thresholds.

past 5 min have consistently exceeded the prespecified criteria, it is also a justification for the system to concurrently reoptimize the ramp metering and arterial signal controls.

Real-Time Deactivation Mechanism. Table 4 shows both the criteria and procedures for assessing if the system should deactivate its real-time operations and stay at the pretimed or time-of-day mode. The core criteria for justifying such deactivations are as follows: (i) the computed ramp metering cycle lengths are consistently equal to the predefined minimum value; (ii) the occupancies detected by the on-ramp detector are consistently lower than a prespecified threshold; (iii) the detected arterial boundary inflow rates are consistently less than a predefined threshold; and (iv) the detected arterial boundary inflow rates exhibit a non-increasing trend.

The Optimization Modules in the RAF-Ramp System

System-Wide Optimization Module

The system-wide optimization module, which integrates the LGB (*30*) and AF-ramp (*1*) models, functions to maximize the total benefits of all motorists on the freeway segments and its neighboring arterial segment based on real-time detected traffic conditions. The module has embedded in it the following sets of constraints: (i) freeway throughput constraints to reflect its relation with the ramp metering cycle; (ii) time-dependent on-ramp constraints to prevent on-ramp overflows; (iii) intersection queue constraints for minimizing intersection queue spillovers; and (iv) intersection flow conservation and signal timing related constraints. The flowchart of the system-wide optimization module is shown in Figure 5.

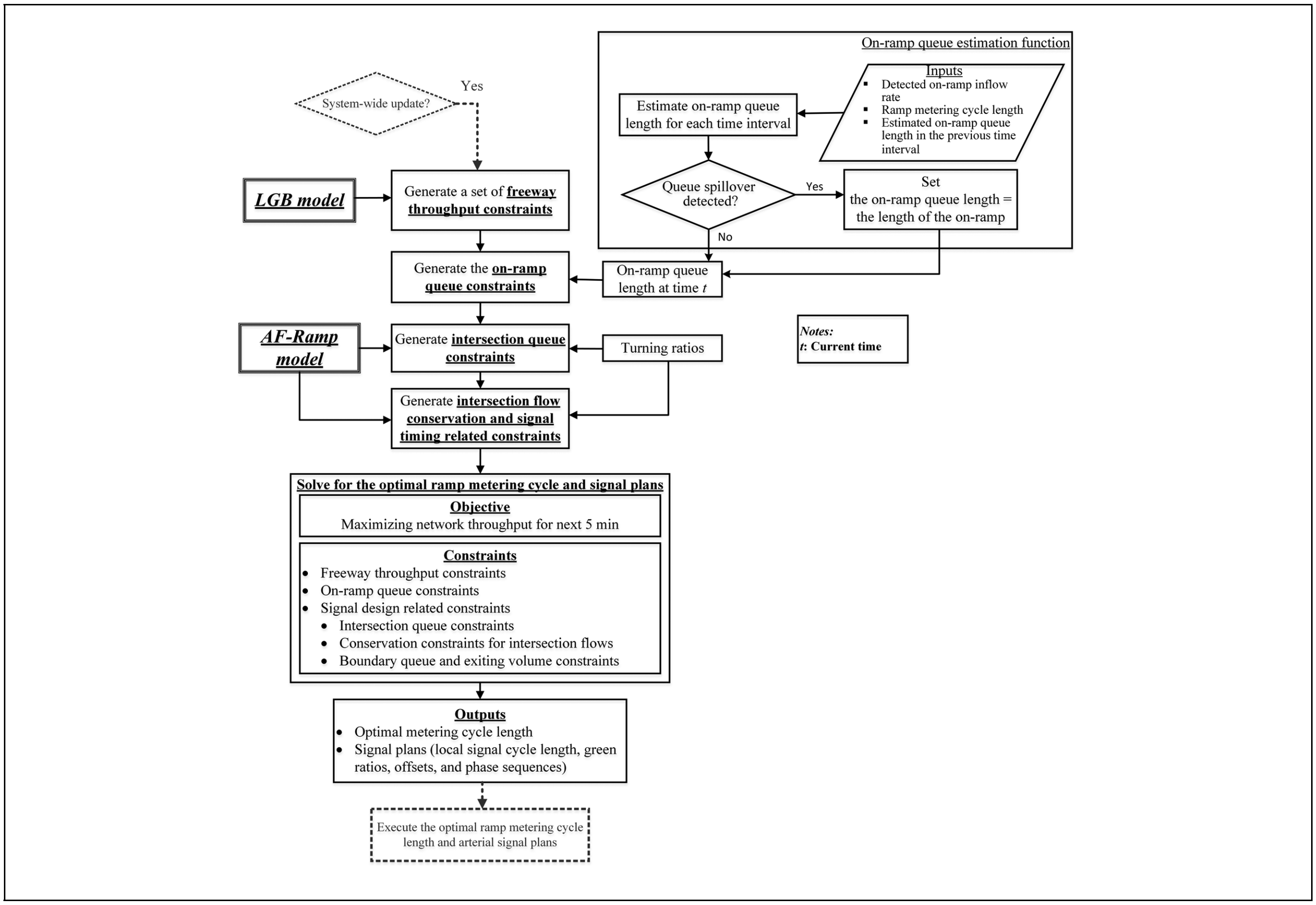

Figure 5. Flowchart of the system-wide optimization module.

Note that the proposed system-wide optimization module is developed with the core concept of the AF-ramp model and some essential enhancements to ensure the effectiveness of its real-time operations. Specifically, the AF-ramp model is designed to maximize the total throughput at both the freeway on-ramp segment and the boundary links within the neighboring local arterial, while ensuring there is no on-ramp queue spillback and progression for multi-path flows on the arterial links based on the historical traffic volume data. To advance the AF-ramp model from a time-of-day mode to real-time operations, the proposed system has incorporated in it the following enhancements: (i) utilizing the LGB model for real-time estimation of freeway capacity; and (ii) establishing the time-dependent on-ramp queue constraints. Those formulations along with key constraints from the AR-ramp model are introduced with the key notations listed in Table 5.

Freeway Throughput Constraints. The first set of constraints, as shown in Equation 3, have been constructed to reflect the relationship between the given ramp cycle length, ω, and the resulting freeway throughput, denoted as $\hat{V}_\omega$. Note that one constraint will be generated for each possible value of C_o so that the system-wide optimization module can precisely select the ramp metering cycle length that yields the highest total throughput for both the freeway segment and the local arterial.

$$V^F = \hat{V}_\omega,\ \text{if } C_o = \omega\ (\forall \omega\ \in [C_{o,min},\ C_{o,\ max}]) \quad (3)$$

where $\hat{V}_\omega$ is the freeway throughput under the given metering cycle, ω, obtained by adding up the throughputs of all lanes of the segment downstream of the on-ramp, $q_{I,J}(k)$ (see Equation 4), which can be explicitly predicted with the LGB model. By integrating the LGB model, nonconvex in nature, to the optimization formulation, one can effectively capture the complex traffic dynamics and also yield a solution sufficiently efficient for real-time needs.

$$\hat{V}_\omega = \sum\nolimits_{k=t+1}^{t+N} \sum\nolimits_{I,J} q_{I,J}(k) \quad (4)$$

Table 5. Key Notations Used in the System-wide Optimization Module

Sets	
Ω	Set of intersection movements heading to the on-ramp
Δ	Set of movements exiting the target network
Φ	Set of movements entering the target network
$D_{I,J}$	The set of lane groups in the adjacent downstream segment connected to lane group J in segment I ($\lvert D_{I,J}\rvert$ is the number of lane groups in $D_{I,J}$)
$S_{I,J}$	The set of lane groups in the adjacent upstream segment connected to lane group J in segment I ($\lvert S_{I,J}\rvert$ is the number of lane groups in $S_{I,J}$)
Parameters	
L_o	On-ramp length (veh)
$s(s_o)$	Saturation flow rate at intersections (the ramp metering point) (vehicles per hour [vph])
t_i	Travel time from intersection i to $i+1$ (in cycle);
$V_{\mu,i}$	Volume demand for movement μ at intersection i (vph)
$f_{\mu,i}$	Lane use factor based on the number of lanes for movement μ at intersection i
$r_{\mu,i}$	Volume ratio of movement μ from arterial at intersection i
$L_{b,i}$, $L_{l,i}$	Bay length and the link length at intersection i (veh)
t_l	Lost time for each signal phase (sec)
T_t	Time duration of the study (hr)
γ	Robustness factor that represents the sensitivity of volume fluctuation to the occurrence of queue spillback
$\dot{n}$	Number of vehicles that are permitted to pass the ramp meter per each green interval
L_I	Length of freeway segment I
H	Average vehicle length (ft)
T	Time interval for updating the traffic state
Z	Number of total time intervals
K	Number of elapsed time intervals
v^m	Minimum speed of freeway vehicles
$\lambda_{I,J}$	Number of lanes in lane group J in segment I
ρ^{jam}	Freeway jam density
ρ_I^C	Critical density of segment I
β_1, β_2	Weighting factors in the objective function
$\eta,\ \tau,\ \upsilon,\ \kappa,\ \phi$	Parameters in the LGB model
Variables for local arterial	
R_i	Number of queueing vehicles outside the target area because of the limited green time (vph)
$l_p(\dot{k})$	Queue length caused by excessive demand at time $\dot{k}$ (veh)
l_e	Queue length caused by arrivals from the upstream intersection in every cycle (veh)
ξ	Reciprocal of the cycle length at the arterial intersections (/sec)
$b_{m,i}$	Local progression bands, that is the duration within which vehicles from traffic path m can traverse intersections i-1 and i without stop (in cycle)
$t^a_{\mu,i}$, $t^b_{\mu,i}$	Start and end of the green phase for downstream movement μ at intersection i
$\tau_{d(m),i}$	Queue clearance time of movement $d(m)$ at intersection i (in cycle)
$l_{\mu,i}$	Queue length for movement μ at intersection i (veh)
V^A	Arterial throughput at the boundary outbound links (vph)
V^a_μ	Actual volume for movement μ at intersection i (vph)
$\Delta\dot{k}$	Duration of one time interval for the local arterial variable updates
Variables for LGB model	
$\alpha_{J,J+1}$	Target density ratio between lane groups J and $J+I$
C_o	The metering cycle length (sec)
$C_{o,min}/C_{o,\ max}$	The minimal/maximal metering cycle length (sec)
$N_{I,J,J+1}(k)$	Number of vehicles changing from lane group J to $J+I$ in segment I at time k. ($J = I, \ldots, G_I - I$; G_I is the number of lane groups in segment I)
$q_{I,J}(k)$	Flow rate of lane group J in segment I at time k (vph)
$q_o(k)$	Outflow rate of the on-ramp at time k (vph);
$\hat{q}_o(k)$	Inflow rate of the on-ramp at time k (vph);
$S_a(k)$	Remaining space in the acceleration lane at time k (veh)
$V_I(.)$	Speed-density relation for segment I
V^F	Freeway throughput at the downstream of the on-ramp segment (vph)
$\hat{V}_\omega$	Freeway throughput under the given metering cycle, ω, obtained by adding up the throughputs of all lanes of the segment downstream of the on-ramp
$v_{I,J}(k)$	Speed of lane group J in segment I at time k (km/h)
$w_o(k)$	Number of vehicles in the on-ramp queue at time k
$\rho_{I,J}(k)$	Density of lane group J in segment I at time k (***before*** receiving lane-changing vehicles)
$\rho^*_{I,J}(k)$	Density of lane group J of segment I at time k (***after*** accommodating lane-changing vehicles)

The key formulations of the LGB model to yield the $q_{I,J}(k)$ under each possible value of metering cycle length are summarized below. A more detailed description of the model can be found elsewhere (*30*).

The number of lane-changing vehicles

$$N_{I,J,J+1}(k) = \begin{cases} \min(L_I \rho_{I,J}(k),\ \eta \lambda_{I+1,J} \lambda_{I+1,J+1} L_{I+1} \frac{\rho_{I+1,J}(k) - \rho_{I+1,J+1}(k)}{\lambda_{I+1,J} + \lambda_{I+1,J+1}} \\ \quad ,\ (\rho^{jam} - \rho_{I,J+1}(k)) L_I),\ \mathit{if}\, \rho_{I+1,J}(k) > \rho_{I+1,J+1}(k) \\ 0,\ \mathit{otherwise} \end{cases} \tag{5}$$

$$N_{I,J,J+1}(k) = \begin{cases} \min(\lambda_{I,J} \lambda_{I,J+1} L_i \frac{\rho_{I,J}(k) - \alpha_{J,J+1} \rho_{I,J+1}(k)}{\lambda_{I,J} \alpha_{J,J+1} + \lambda_{I,J+1}}, \\ (\rho^{jam} - \rho_{I,J+1}(k)) L_I),\ \mathit{if}\, \rho_{I,J}(k) > \alpha_{J,J+1} \rho_{I,J+1}(k) \\ 0,\ \mathit{otherwise} \end{cases} \tag{6}$$

Flow rate and density calculation

$$\rho_{I,J}(k+1) = \begin{cases} \rho^*_{I,J}(k) + \frac{T}{L_I \lambda_{I,J}} \left[\frac{\lambda_{I,J}}{\lambda_{I-1,J}} q_{I-1,J}(k) - q_{I,J}(k) \right],\ \mathit{if}\ \lambda_{I,J} \leq \lambda_{I-1,J} \\ \rho^*_{I,J}(k) + \frac{T}{L_I \lambda_{I,J}} \left[\left[\sum_{m \in S_{I,J}} \lambda_{I-1,m} q_{I-1,m}(k) \right] - q_{I,J}(k) \right],\ \mathit{if}\ \lambda_{I,J} > \lambda_{I-1,J} \end{cases} \tag{7}$$

$$q_{I,J}(k) = \lambda_{I,J} \rho^*_{I,J}(k) v_{I,J}(k) \tag{8}$$

$$\rho^*_{I,J}(k) = \rho_{I,J}(k) + \frac{N_{I,J-1,J}(k) - N_{I,J,J+1}(k)}{L_I \lambda_{I,J}} \tag{9}$$

$$q_o(k) = \min\{(\hat{q}_o(k) + \frac{w_o(k)}{T/3600}), \frac{2 * \dot{n} * S_o}{\omega}, \frac{S_a(k)}{T/3600} \tag{10}$$

Speed update

$$\begin{aligned} v_{I,J}(k+1) = & \max\{v^m, v_{I,J}(k) + \frac{T}{\tau} \left[V_I \left(\rho^*_{I,J}(k) \right) - v_{I,J}(k) \right] \\ & + \frac{T}{L_I} v_{I,J}(k) [\frac{\sum_{m \in S_{I,J}} (v_{I-1,m}(k))}{|S_{I,J}|} - v_{I,J}(k)] - \frac{\upsilon T}{\tau L_I} \frac{[\frac{\sum_{w \in D_{I,J}} (\rho^*_{I+1,w}(k))}{|D_{I,J}|} - \rho^*_{I,J}(k)]}{\rho^*_{I,J}(k) + \kappa} \\ & - \frac{\phi \max(v_{I,J}(k) - v_{I,J-1}(k), 0) N_{I,J-1,J}(k)}{L_I \lambda_{I,J} \rho^C_I} \} \end{aligned} \tag{11}$$

Equations 5 and 6 are developed to calculate the number of lane-changing vehicles between lane groups within the on-ramp segments and the downstream segments, respectively. Equation 7 formulates the dynamics of density evolution for each lane group using the flow conservation relation, which utilizes the lane group density after receiving the lane-changing vehicles ($\rho^*_{I,J}(k)$) and flow rate ($q_{I,J}(k)$) specified in Equations 8 and 9. The on-ramp outflow rate is determined by Equation 10. In addition, Equation 11 is specified to reflect the speed dynamics for each lane group within each segment.

Note that a new set of Equation 3 should be produced, to reflect the real-time relation between freeway throughput and the ramp metering cycle, based on the output of the LGB model if the system-wide optimization is needed.

On-Ramp Queue Constraints. The set of constraints is developed to ensure that the on-ramp queues under the ramp metering control would not exceed the ramp's length during the entire control period. Conceivably, the ramp queue consists of residual queues because of the difference between the on-ramp's entering and exiting flow rates and the arriving vehicles discharged per cycle from those intersections within the control zone. One can formulate Equation 12 to calculate the former at the end of the next control interval and let the latter be expressed with Equation 13.

$$l_p(\dot{k}+1)=\max(w_o(\dot{k})+\left(\sum\nolimits_{\mu\in\Omega}V_\mu^a-s_o r_o\right)\cdot\frac{\Delta\dot{k}}{3600},0) \quad (12)$$

$$l_e(\dot{k}+1)=\sum\nolimits_{\mu\in\Omega}V_\mu^a/3600\xi \quad (13)$$

$$w_o(\dot{k})= \max(\min\left(w_o(\dot{k}-1)+\frac{\Delta\dot{k}}{3600}*(\hat{q}_o(\dot{k}-1)-q_o(\dot{k}-1)),\frac{L_o}{H}\right),0) \quad (14)$$

where $l_p(\dot{k}+1)$, denoting the on-ramp queue length caused by excessive on-ramp flows at the end of time interval ($\dot{k}+1$), is to be updated by the on-ramp queue estimation function when no queue spillover is detected by the on-ramp detector, as shown in Equation 14. If a queue spillover is detected, then $w_o(\dot{k})$ will be set to (L_o/H). Note that such queue length $l_p(\dot{k}+1)$ may decrease during the next control interval, if the on-ramp arriving flow rate is lower than the metering rate. The right-hand side of Equation 13 is to sum up all traffic flows entering the on-ramp during one signal cycle from the intersections. Note that the length of time intervals in Equations 12 to 14 may be different from those in Equations 4 to 11.

To ensure that the on-ramp queue length would not increase rapidly at the start of the peak periods, the allowed upper bound for the on-ramp queue length should be time-dependent, based on the ratio of the elapsed time over the total period, as expressed in Equation 15.

$$l_p(\dot{k})\leq\min((\tfrac{K}{Z}\left(L_o/H-l_e(\dot{k})\right),\left(L_o/H-l_e(\dot{k})\right))$$

In Equation $15\left(L_o/H-l_e(\dot{k})\right)$ is specified to calculate the available space for the vehicle queues caused by excessive on-ramp flows.

Intersection Queue Constraints. To ensure that the proposed ramp control will not cause queue spillback at those intersections feeding flows to the freeway, the proposed system adopts the formulations in the AF-ramp model to estimate the number of vehicles stopping at the intersections within the ramp's affected area. Figure 6 illustrates the local progression band for one traffic path on an arterial link, where the specially-designed signal plan to coordinate with ramp control can ensure that the intersection queues will not overflow from their designated links.

The intersection queue constraints can be summarized as below:

$$b_{m,i}=\min\left(t^b_{d(m),i},t^b_{u(m),i-1}+t_{i-1}\right)-\max\left(t^a_{d(m),i}+\tau_{d(m),i},t^a_{u(m),i-1}+t_{i-1}\right) \quad (16)$$

$$l_{\mu,i}=\sum_{d(m)=\mu}V^a_{u(m),i-1}r_{d(m),i}\left(g_{u(m),i-1}-b_{m,i-1}\right)f_{d(m),i}/3600\xi,\quad \mu=\text{through or left}-\text{turn} \quad (17)$$

$$l_{\mu,i}\frac{s}{s-V_{\mu,i}f_{\mu,i}}\times\gamma\leq L_{b,i} \quad (18)$$

$$l_{\mu,i}\frac{s}{s-V_{\mu,i}f_{\mu,i}}\times\gamma\leq L_{l,i} \quad (19)$$

$$\tau_{\mu,i}=l_{\mu,i}\frac{3600\xi}{s-V_{\mu,i}f_{\mu,i}} \quad (20)$$

where Equation 16 calculates the local band between two intersections for traffic stream m, that is, a period during which vehicles would pass two adjacent intersections without encountering red phases; Equation 17 calculates queue lengths on the left-turn lanes and through lanes of the arterial links based on the local bandwidths; Equations 18 and 19 function to ensure that the maximum queue length during a cycle would not exceed the turning bay or the link length; and Equation 20 estimates the queue discharging time. Note that the traffic volume in the above equations is updated in real time based on the traffic detected at the boundary links of the network.

The remaining essential yet fundamental formulations, including the intersection flow conservation equation and green time allocation constraints, are identical to those in the AF-ramp model (*1*).

Objective Function. Note that the system-wide optimization module is focused on maximizing the total throughput for the freeway and the local arterial. Furthermore, those queueing vehicles that may not be able to enter the control area because of the shorter cycle length and green ratio shall result in a penalty to the objective function since these vehicles would incur excessive delay if not properly discharged. Therefore, the objective function of the system-wide control model can be expressed as follows,

$$\text{Max } V^F+\beta_1V^A-\beta_2\sum\nolimits_{i\in\varpi}R_i$$

s.t.

Freeway throughput constraint: Equation 3
On-ramp queue constraints: Equations 12 to 15
Intersection queue constraints: Equations 16 to 20
Intersection flow conservation and signal timing related constraints (*1*).

With the above objective function and constraints, the optimization model can be formulated with mixed integer linear programming, and thus can be solved with various existing commercial packages.

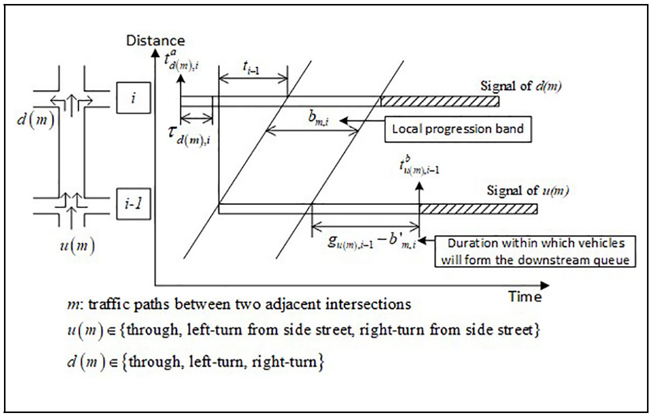

Figure 6. Local paths between two adjacent intersections near the on-ramp.

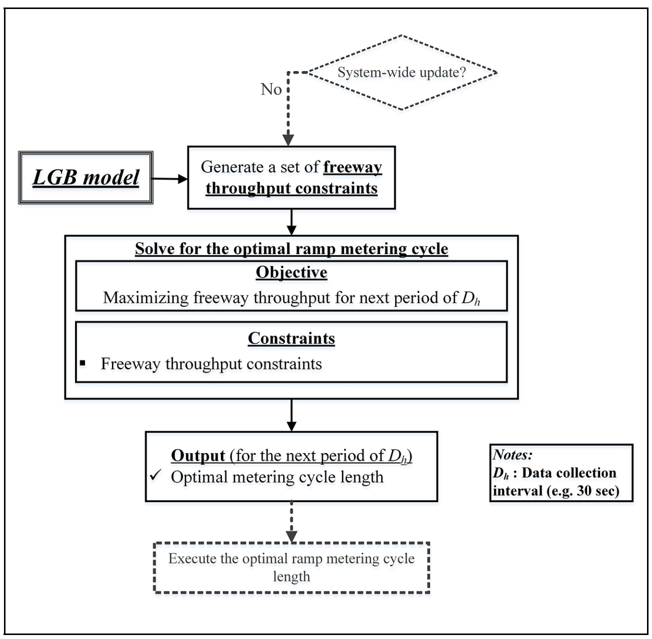

Figure 7. Flowchart of the ramp metering optimization module.

Ramp Metering Optimization Module

The flowchart of the ramp metering optimization module for the proposed system is shown in Figure 7. When reoptimizing the ramp control alone is justified at Stage 3 of the operations, its primary control objective is to maximize the freeway throughput. Following the logic of the system-wide optimization module, the LGB model will be adopted to predict the freeway throughputs under the set of candidate metering cycle lengths (i.e., between maximal and minimal metering cycle lengths), as expressed with the right-hand side terms of Equation 3. The complete ramp metering optimization module is shown below,

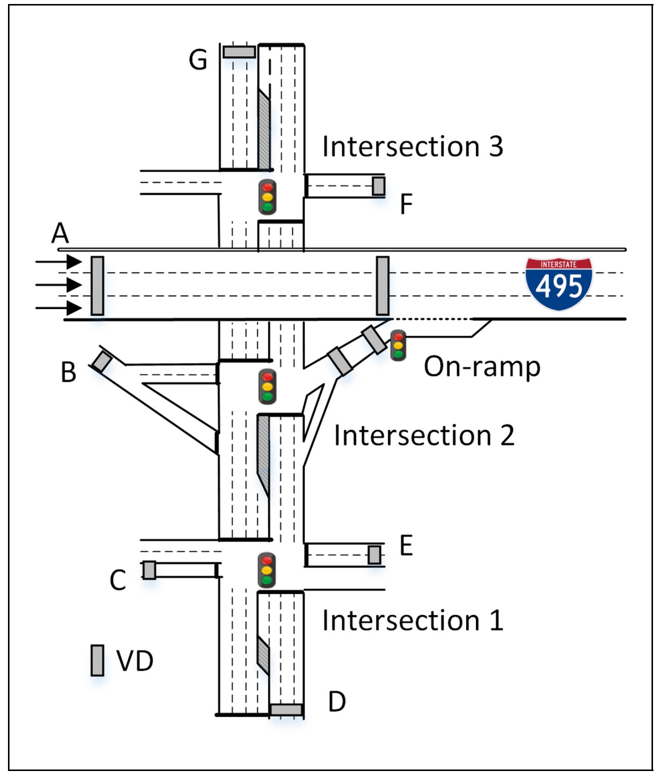

Figure 8. Geometric features of the test site and locations of its detectors.

$$\text{Max} V^F$$

$s.t.$

Freeway throughput constraint: Equation 3

where V^F is the freeway throughput.

Case Study

The case study is designed to demonstrate the effectiveness of the proposed RAF-ramp system in (i) smoothing the freeway traffic conditions; (ii) preventing overflows at the on-ramp and local arterial's turning bays; and (iii) maximizing the total throughput as well as minimizing the total delay for the control area. The proposed system will also be compared with a widely-applied real-time ramp metering model, ALINEA/Q (*7*), and its pre-timed version, the AF-ramp model (*1*), with respect to multiple measures of effectiveness (MOEs), including average speeds, maximal on-ramp and intersection queue lengths, and total throughputs as well as delays.

Test Site and Experimental Design

The freeway mainline merging segment at Exit 36 of I-495 Inner Loop in Bethesda, Maryland, U.S.A., and its neighboring local intersections are adopted as the study site. Figure 8 illustrates the test site's geometric features and the locations of its vehicle detectors. The average

Table 6. Time-Varying Flow Rates Under Three Experimental Scenarios

		Unit: vehicles per hour						
Time (seconds)	Scenario	A (3 lanes)	B (1 lane)	C (1 lane)	D (3 lanes)	E (2 lanes)	F (2 lanes)	G (3 lanes)
0–600	1	3000	500	400	1000	800	250	800
	2	3150						
	3	2850						
600–1500	1	5000	500	400	1800	800	250	1200
	2	5250						
	3	4750						
1500–2400	1	4200	500	400	1200	800	250	1200
	2	4410						
	3	3990						
2400–3000	1	5000	500	400	1800	800	250	1200
	2	5250						
	3	4750						
3000–3600	1	3500	500	400	1000	800	250	800
	2	3675						
	3	3325						

Table 7. Intersection Turning Ratios Under Three Experimental Scenarios

	Northbound			Southbound			Eastbound			Westbound		
Intersection	L	T	R	L	T	R	L	T	R	L	T	R
1	0.01	0.98	0.01	0.04	0.95	0.01	0.92	0.04	0.04	0.39	0.01	0.6
2	na	0.8	0.2	0.25	0.75	na	0.2	0	0.8	na	na	na
3	0.14	0.86	na	na	0.8	0.2	na	na	na	0.5	0	0.5

Note: L = left turn; R = right turn; T = through. na = not applicable.

flow rates and the intersection turning ratios of three experimental scenarios are shown in Tables 6 and 7, respectively. For evaluation of the robustness of the proposed system's performance, the freeway's mainline flow rates in Scenarios 2 and 3 are set to be 5% higher and 5% lower than those of Scenario 1, respectively. The phasing plans for all neighboring local intersections are prespecified and shown in Table 8, but their green splits, as well as phase sequences, are to be optimized with the proposed system. In addition, the green splits, phase sequences, and metering rates of the fixed-time plan optimized with average flow rates between 600 and 3,000 s in Scenario 1 are shown in Table 9.

Note that the metering control in the case study is operated with the practice of two cars per green interval. The time interval of 30 s is adopted for updating the ramp metering cycle and 5 min for the system-wide optimization that includes local signal plans and offsets.

Design of the Simulator for Real-Time Simulation Analysis

Figure 9 shows the simulator for simulating the proposed control system under real-time operations, where its traffic simulation module is built with VISSIM 10 (PTV, (*31*)), and the control module, including the LGB model, is coded with VB.NET to reflect its interactions with simulated traffic conditions via the VISSIM COM interface. All vehicle detectors, needed for real-time control and system evaluation, are shown in Figure 8. All such detected traffic information, as shown in Figure 9, will be transmitted to the RAF-ramp system's simulator constantly through the COM interface for predicting the traffic states and optimizing the control strategies for the projected time horizon.

The optimization modules are solved with Gurobi 9 (Gurobi Optimization, (*32*)) on a Windows 10 desktop with an Intel Core i7-9700 processor and 16 GB RAM. The computation times for the system-wide optimization and ramp metering update modules to reach optimality are less than 10 s and 1 s, respectively. Moreover, with regard to solution quality, optimality is considered to be achieved in Gurobi when the percentage difference between the primary objective upper bound and dual objective lower bound is lower than 0.01%. The resulting MOEs for performance comparison, are measured directly from the simulator's output.

Table 8. Phase Plans for Three Intersections Within the Control Area

Intersection	Phase ID 1	2	3	4
1				
2				na
3				na

Note: na = not available.

Table 9. The Fixed-time Signal Plan and Metering Rate

Intersection	Phase 1	2	3	4	Offset
1	19s	48s	30s	23s	0
2	26s	54s	40s	na	0
3	30s	61s	29s	na	0

Cycle length: 120 s
Metering rate: 0.33 (the metering control in the case study will be under 2-cars-per-green interval)
Note: na = not available.

Performance Under the Medium-Volume Scenario (Scenario 1)

Figures 10 to 12 show the average lane speeds on the freeway's merging segment under the RAF-ramp, ALINEA/Q, and AF-ramp, respectively, under Scenario 1. Since the traffic on the outermost lane of the freeway merging area is affected most by the merging flows, Figure 13 shows the comparisons of the average speeds on the outermost lane (i.e., lane 1) under Scenario 1 under all three control strategies. Figure 14 illustrates the resulting distributions of queue lengths associated with each intersection approach under this scenario.

As shown in Figure 10, the lane speeds under the proposed RAF-ramp system are constantly above 40 km/h. However, this traffic scenario frequently triggers the queue override function in ALINEA/Q and causes the freeway mainline traffic to break down. For example, speeds on the outermost lane are mostly below 40 km/h during the periods of executing the queue override function, as shown in Figure 11. The performance results from this experimental scenario seem to confirm the benefits of having optimal coordination between the on-

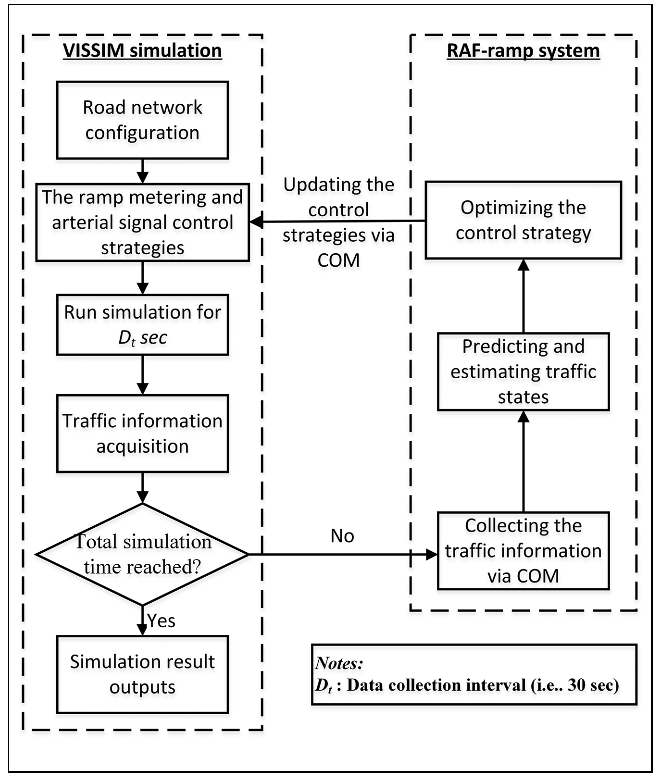

Figure 9. Structure of the simulator for simulating real-time operations of the real-time arterial-friendly ramp (RAF-ramp) control system.

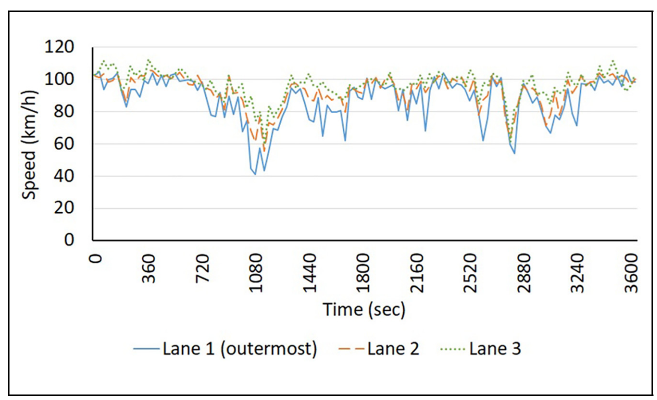

Figure 10. Average lane speeds on the freeway's merging segment under the real-time arterial-friendly ramp (RAF-ramp) control (Scenario 1).

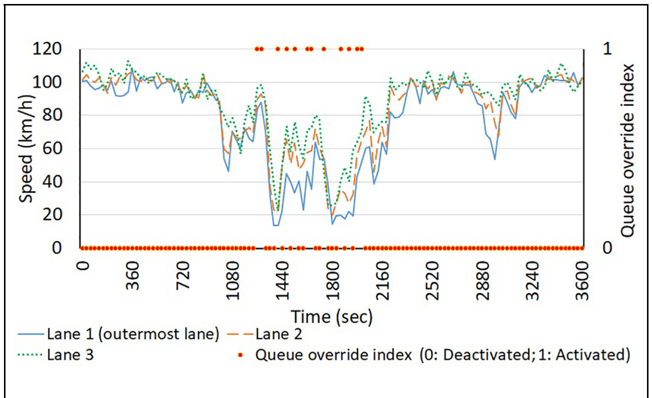

Figure 11. Average lane speeds on the freeway's merging segment under ALINEA/Q control (Scenario 1).

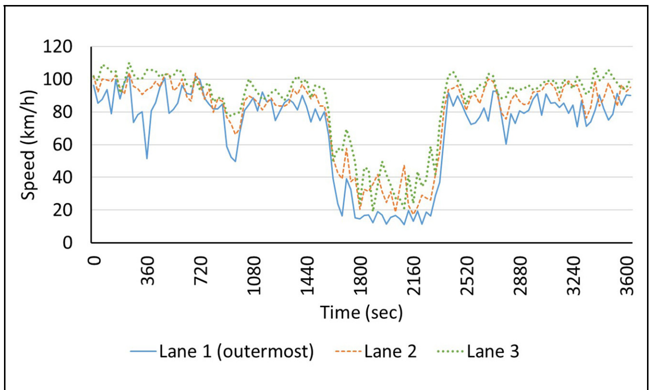

Figure 12. Average lane speeds on the freeway's merging segment under the arterial-friendly local ramp (AF-ramp) system (Scenario 1).

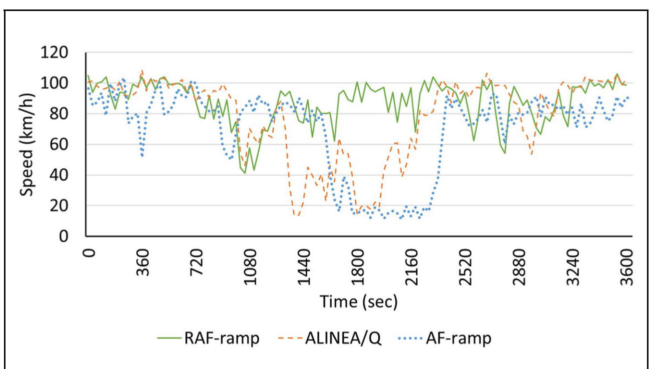

Figure 13. Comparison of average speeds of lane 1 (outermost) on the freeway's merging segment (Scenario 1).

ramp metering and its neighboring intersections. It is noticeable that the queues on all links under RAF-ramp, ALINEA/Q, and AF-ramp controls do not spill back

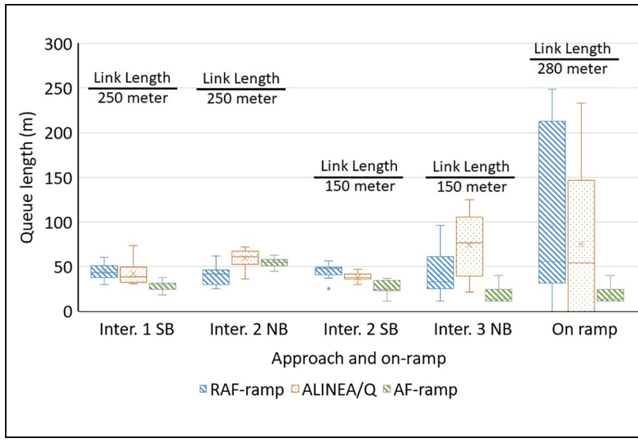

Figure 14. Distributions of queue lengths at different intersection approaches (Scenario 1).

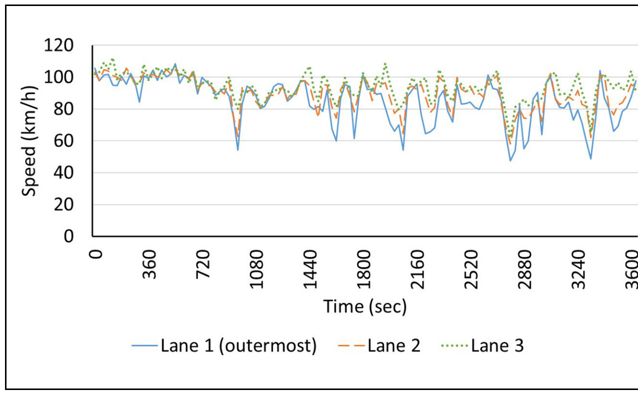

Figure 15. Average lane speeds on the freeway's merging segment under real-time arterial-friendly ramp (RAF-ramp) control (Scenario 2).

to neighboring intersections under this scenario (see Figure 14).

Performance Under the High-Volume Experimental Scenario (Scenario 2)

Figures 15 to 19, respectively, show the freeway's lane speeds and the distributions of queue lengths with the RAF-ramp, ALINEA/Q, and AF-ramp controls under Scenario 2. The average lane speeds on the target freeway segment with the proposed system remain above 40 km/h (see Figure 15) under such a high-volume traffic condition. In contrast, the speeds on the freeway's outermost lane drop below 30 km/h during the period when ALINEA/Q control inevitably executes its queue override function (see Figure 16). In addition, the pretimed control cannot prevent speed drop, as shown in Figure 17. Figure 18 presents the comparison on lane 1's speeds under the three control strategies. Furthermore,

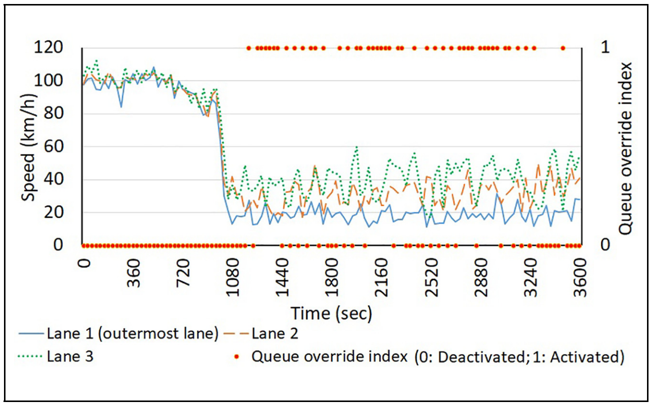

Figure 16. Average lane speeds on the freeway's merging segment under the ALINEA/Q control (Scenario 2).

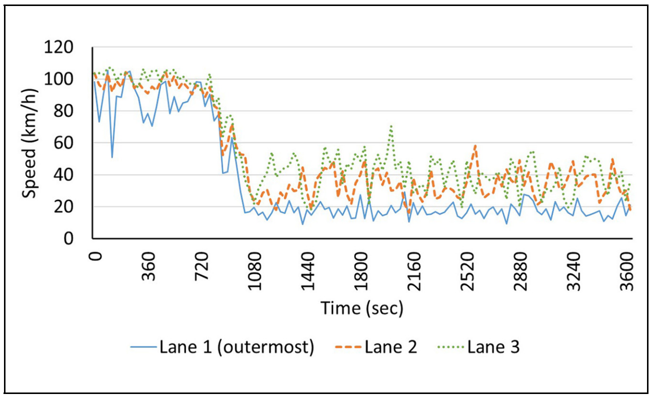

Figure 17. Average lane speeds on the freeway's merging segment under the arterial-friendly local ramp (AF-ramp) system (Scenario 2).

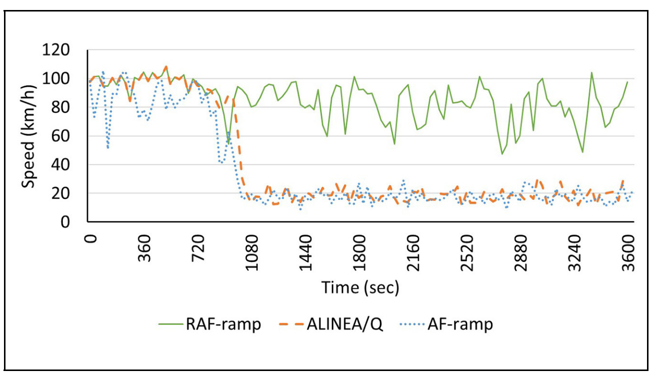

Figure 18. Comparison of average speeds of lane 1 (outermost) on the freeway's merging segment (Scenario 2).

the total throughput from the control area under the RAF-ramp system in Scenario 2 is 5.34% (6,031 vehicles versus 5,725 vehicles) higher than that with ALINEA/Q.

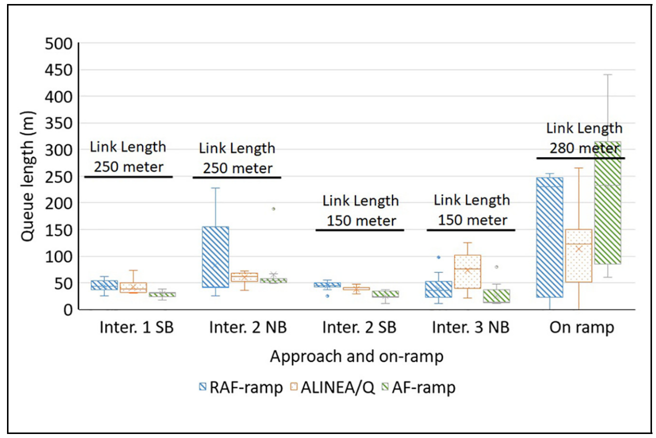

Figure 19. Distributions of queue lengths at different intersection approaches (Scenario 2).

In brief, the performance results under Scenario 2 further support the benefits of integrating on-ramp metering with local signal controls as modeled in the RAF-ramp system. Such benefits over ALINEA/Q control with ramp metering only are likely to be more pronounced in higher volume scenarios, as reflected in the differences of MOEs between Scenario 1 and Scenario 2. Note that all arterial links, as with Scenario 1, do not experience any queue spillback during the entire experimental period under both controls (see Figure 19).

Performance Under the Light Volume Scenario (Scenario 3)

Figures 20 to 24 show the freeway's lane speeds and the distributions of queue lengths under the scenario of relatively low freeway traffic. As expected, under such a low-volume traffic scenario, all three control systems can maintain average lane speeds above 40 km/h (see Figures 20 to 22). Figure 23 shows the speed comparisons of the outermost lane (i.e., lane 1) with all three control strategies under this scenario. The MOEs for such a traffic scenario can further support the advantage of always coordinating the ramp metering control with its neighboring intersections which accommodate traffic flows to the freeway. As with the previous two scenarios, the intersection queue lengths with the proposed RAF-ramp under Scenario 3 are constantly shorter than the link lengths (see Figure 24).

Network-wide Delay Under All Volume Scenarios

Table 10 shows the total delays of the entire network under the control with the two real-time and one pretimed ramp metering strategies, demonstrating that the proposed RAF-ramp outperforms the other two controls

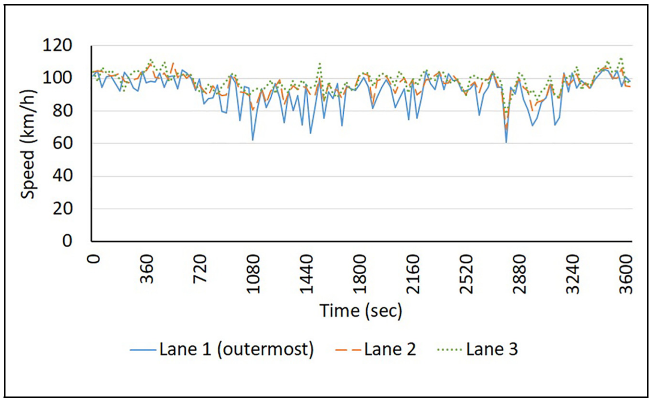

Figure 20. Average lane speeds turning on the freeway's merging segment under real-time arterial-friendly ramp (RAF-ramp) control (Scenario 3).

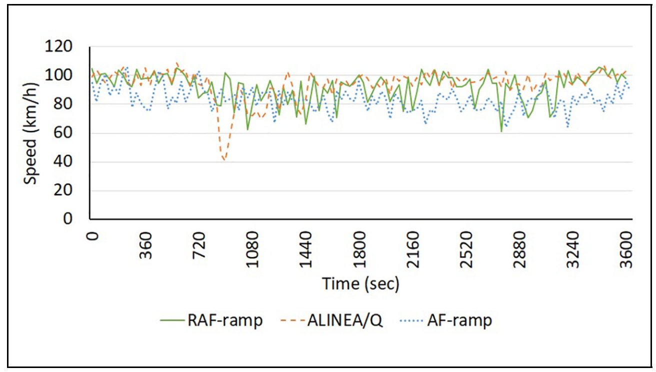

Figure 23. Comparison of average speeds of lane 1 (outermost) on the freeway's merging segment (Scenario 3).

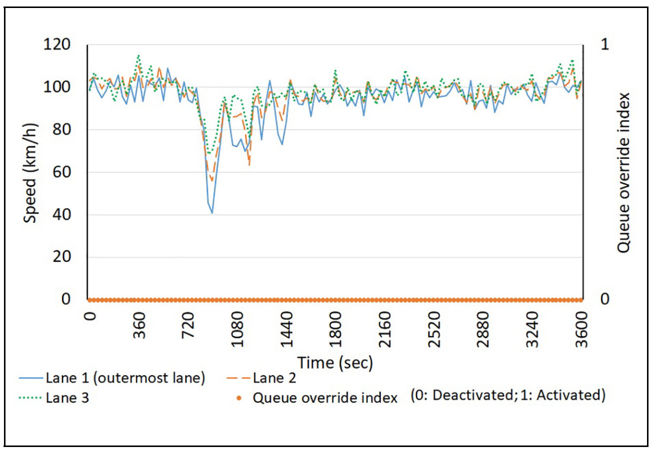

Figure 21. Average lane speeds on the freeway's merging segment under ALINEA/Q control (Scenario 3).

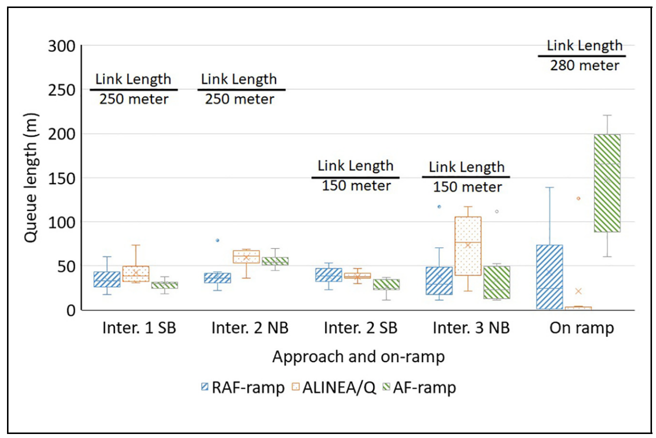

Figure 24. Distributions of queue lengths at different intersection approaches (Scenario 3).

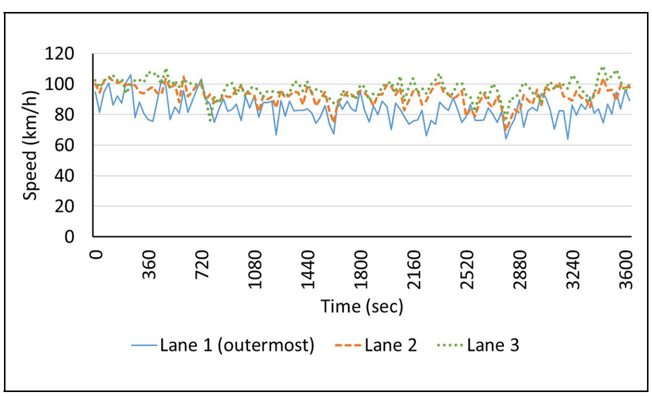

Figure 22. Average lane speeds on the freeway's merging segment under the arterial-friendly local ramp (AF-ramp) system (Scenario 3).

in all three scenarios, especially in medium- and high-volume scenarios (i.e., Scenarios 1 and 2). Such improvement mainly come from the freeway mainline, as evidenced by the total delays on the freeway mainline and on-ramp under Scenarios 1 and 2 shown in Figure 25. For example, under Scenario 2 of high-volume traffic conditions, the RAF-ramp system can achieve up to 63.27% and 67% improvements, compared with ALINEA/Q and AF-ramp, respectively. In the same scenario, the total delay on the freeway mainline under RAF-ramp control is 8.1 vehicle hours, significantly lower than those under ALINEA/Q and the AF-ramp system (i.e., 115.4 and 118.5 vehicle hours, respectively), as shown in Figure 25*b*.

Moreover, the benefits of the RAF-ramp system tend to increase with the freeway's traffic volume. As shown in Table 10, when freeway volume increases by 5% (i.e., from Scenario 1 to Scenario 2), the total delay under the proposed RAF-ramp increases by 28.96% (from 46.83 vehicle hours in Scenario 1 to 60.39 vehicle hours in Scenario 2), considerably lower than the increments of

Table 10. Total Delays of the Proposed Real-Time Arterial-Friendly Ramp (RAF-Ramp), ALINEA/Q, and arterial-friendly local ramp (AF-Ramp)

Control strategy	Scenario 1	Scenario 2	Scenario 3	Unit: vehicle hours Increment[a] (Scenario 2 versus 1) (%)
RAF-ramp system	46.83	60.39	40.33	28.96
ALINEA/Q	59.40	164.42	43.15	176.80
AF-ramp system	68.50	183.0	51.30	167.15
Improvement[b]				
Compared with ALINEA/Q (%)	21.16	63.27	6.54	na
Compared with AF-ramp (%)	31.64	67	21.38	na

[a]Increment = (total delay of the control approach under Scenario 2 – total delay of the control approach under Scenario 1)/(total delay of the control approach under Scenario 1) × 100%.
[b]Improvement = (total delay of the compared control approach – total delay of the proposed RAF-ramp system)/(total delay of the compared control approach) × 100%.
Note: na = not applicable

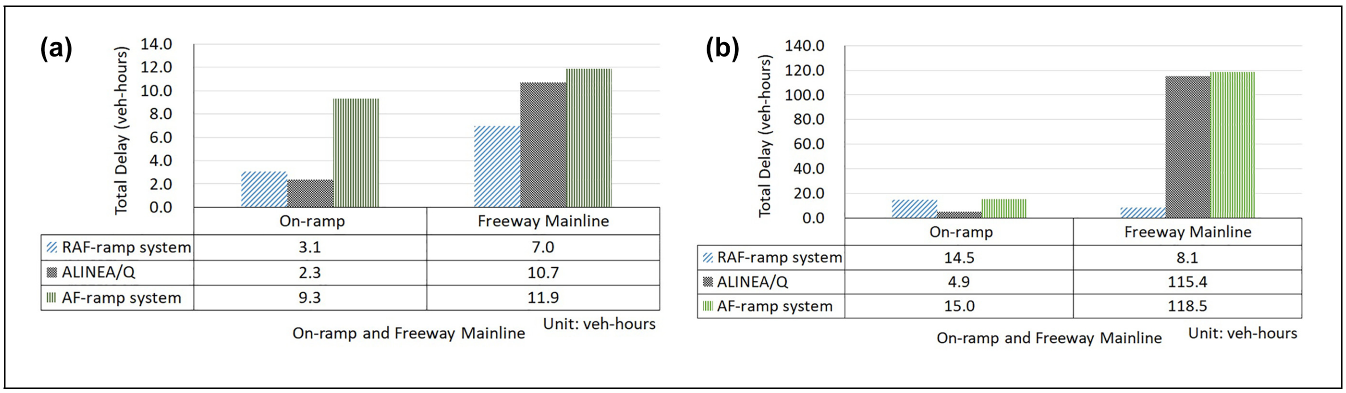

Figure 25. Total delays on the freeway mainline and on-ramp under two different controls: (*a*) Scenario 1 and (*b*) Scenario 2.

176.8% and 167.15% when with the ALINEA/Q and the AF-ramp controls, respectively.

In brief, the proposed RAF-ramp system, by optimally coordinating the ramp metering control with signals at its neighboring intersections, offers the promise to outperform its pre-timed version (i.e., AF-ramp system) and the ALINEA/Q, designed solely for optimizing the ramp metering cycle, with respect to the total network delays, total throughput, and freeway speeds.

Conclusion

To transform the relationship between the motorists on the freeway and its neighboring arterials from competition to coordination in contending with recurrent congestion in the interchange area because of excessive on-ramp volume, this study has proposed the RAF-ramp control system, which can maximize the total benefits for both the freeway segment and arterial intersections within the same control area with the optimally coordinated dynamical ramp metering and multi-path local signal progression control. To sufficiently respond to the freeway traffic dynamics yet maintain the stability of local signal control, the proposed system will execute its system-wide update of both the ramp metering cycle and coordinated signal plans only if the local dynamic ramp control under the objective of maximizing the freeway throughput over the projected time horizon will inevitably cause queue overflows.

The system-wide optimization module, by integrating the predicted freeway traffic conditions from the LGB module with the coordinated signal and ramp relations in the AF-ramp models, can concurrently produce the optimized ramp metering cycle and neighboring intersections' cycle lengths, green splits, phase sequences, and offsets, with the objective to maximize the total system throughput without ramp queue spillback.

The results of extensive simulation experiments have confirmed that the proposed system under three experimental traffic scenarios can produce the optimal control strategies that can effectively utilize the freeway's weaving capacity and also best coordinate neighboring intersections' signal controls to prevent on-ramp queue spillbacks. The results of performance comparison with the AF-ramp and a benchmark real-time ramp control model have justified the need to adopt RAF-ramp under fluctuating traffic conditions, and also the benefits to integrating those intersections feeding traffic to an on-ramp into the same control system. With optimized coordination between the ramp metering cycle and local signal plans, an interchange can best keep its freeway segment's throughput at the weaving capacity while ensuring no ramp overflows with its arriving traffic regulated responsively by the local signals.

Further studies along this line will focus on expanding the proposed system to account for the impacts of off-ramp flows on the congestion on both the freeway and its neighboring arterial and thus develop a full interchange-based real-time traffic control system. Another natural extension of this study is to expand the coordinated local ramp and intersection controls to a corridor-wide traffic management system that covers multiple freeway segments and local arterials significantly affected by the on- and off-ramp traffic.

Author Contributions

The authors confirm contribution to the paper as follows: study conception and design: Y.-Y. Chen, Y. Cheng, G.-L. Chang; data collection: Y.-Y. Chen, Y. Cheng; analysis and interpretation of results: Y.-Y. Chen; draft manuscript preparation: Y. Cheng, Y.-Y. Chen, G.-L. Chang. All authors reviewed the results and approved the final version of the manuscript.

Declaration of Conflicting Interests

The author(s) declared no potential conflicts of interest with respect to the research, authorship, and/or publication of this article.

Funding

The author(s) received no financial support for the research, authorship, and/or publication of this article.

ORCID iDs

Yao Cheng https://orcid.org/0000-0002-0513-0272
Yen-Yu Chen https://orcid.org/0000-0003-0316-0694

References

1. Cheng, Y., and G. L. Chang. Arterial-Friendly Local Ramp Metering Control Strategy. *Transportation Research Record: Journal of the Transportation Research Board*, 2021. 2675: 67–80.
2. Piotrowicz, G., and J. Robinson. *Ramp Metering Status in North America*. FHWA (No. DOT-T-95-17). Federal Highway Administration, U.S. Department of Transportation, Washington, D.C., 1995.
3. Masher, D. P., D. W. Ross, P. J. Wong, P. L. Tuan, H. M. Zeidler, and S. Petracek. *Guidelines for Design and Operation of Ramp Control Systems*. Stanford Research Institute, Menlo Park, CA, 1975.
4. Papageorgiou, M., H. Hadj-Salem, and J. M. Blosseville. ALINEA: A Local Feedback Control Law for On-Ramp Metering. *Transportation Research Record: Journal of the Transportation Research Board*, 1991. 1320: 58–67.
5. Papageorgiou, M., H. Hadj-Salem, and F. Middelham. ALINEA Local Ramp Metering: Summary of Field Results. *Transportation Research Record: Journal of the Transportation Research Board*, 1997. 1603: 90–98.
6. Zhang, H. M., and S. G. Ritchie. Freeway Ramp Metering Using Artificial Neural Networks. *Transportation Research Part C: Emerging Technologies*, Vol. 5, No. 5, 1997, pp. 273–286.
7. Smaragdis, E., and M. Papageorgiou. Series of New Local Ramp Metering Strategies. *Transportation Research Record: Journal of the Transportation Research Board*, 2003. 1856: 74–86.
8. Xu, J., W. S. Yu, and F. Y. Wang. Ramp Metering Based on Adaptive Critic Designs. *Proc., IEEE Intelligent Transportation Systems Conference*, Toronto, ON, IEEE, New York, 2006, pp. 1531–1536.
9. Hou, Z., J. X. Xu, and J. Yan. An Iterative Learning Approach for Density Control of Freeway Traffic Flow via Ramp Metering. *Transportation Research Part C: Emerging Technologies*, Vol. 16, No. 1, 2008, pp. 71–97.
10. Paesani, G. F. System Wide Adaptive Ramp Metering in Southern California. Presented at ITS America 7th Annual Meeting and Exposition: Merging the Transportation and Communications Revolutions, Intelligent Transportation Society of America (ITS America), Washington, D.C., 1997.
11. Papageorgiou, M., J. M. Blosseville, and H. Haj-Salem. Modelling and Real-Time Control of Traffic Flow on the Southern Part of Boulevard Périphérique in Paris: Part II: Coordinated On-Ramp Metering. *Transportation Research Part A: General*, Vol. 24, No. 5, 1990, pp. 361–370.
12. Papamichail, I., M. Papageorgiou, V. Vong, and J. Gaffney. Heuristic Ramp-Metering Coordination Strategy Implemented at Monash Freeway, Australia. *Transportation Research Record: Journal of the Transportation Research Board*, 2010. 2178: 10–20.
13. Wattleworth, J. A. Peak-Period Analysis and Control of a Freeway System. No. Hpr 1/4/. Texas Transportation Institute, College Station, TX, 1965.
14. Wang, Y., K. A. Perrine, and Y. Lao. *Developing an Area-Wide System for Coordinated Ramp Meter Control*. No. TNW2008-11. Transportation Northwest (Organization), Seattle, WA, 2008.
15. Lipp, L. E., L. J. Corcoran, and G. A. Hickman. *Benefits of Central Computer Control for Denver Ramp-Metering System*. No. 1320. Transportation Research Board, Washington, D.C., 1991.
16. Liu, J. C. S., J. L. Kim, Y. Chen, Y. Hao, S. Lee, T. Kim, and M. Thomadakis. *An Advanced Real-Time Ramp Metering System (ARMS): The System Concept*, Vol. 1232, No. 24. Texas Transportation Institute, Austin, TX, 1994.

17. Shaaban, K., M. A. Khan, and R. Hamila. Literature Review of Advancements in Adaptive Ramp Metering. *Procedia Computer Science*, Vol. 83, 2016, pp. 203–211.
18. Lu, X. Y., C. J. Wu, and X. Y. Lu. Field Test Implementation of Coordinated Ramp Metering Control Strategy: A Case Study on SR-99N. *Proceedings of the Transportation Research Board Meeting 96th Annual Meeting*. 2018.
19. Zhang, M., T. Kim, X. Nie, W. Jin, L. Chu, and W. Recker. *Evaluation of On-Ramp Control Algorithms*. California PATH Research Report UCB-ITS-PRR-2001-36. University of California Berkeley, CA, 2001.
20. Kattan, L., and M. S. Saidi. *Design and Evaluation of Adaptive Coordinated Ramp Control Strategies on Deerfoot Trail Using Paramics Microsimulation*. Final Report. University of Calgary, Alberta, Canada, 2011.
21. Gordon, R. L. Algorithm for Controlling Spillback from Ramp Meters. *Transportation Research Record: Journal of the Transportation Research Board*, 1996. 1554: 162–171.
22. Sun, X., and R. Horowitz. A Localized Switching Ramp-Metering Controller with a Queue Length Regulator for Congested Freeways. *Proc., American Control Conference*, Portland, OR, IEEE, New York, June 8–10, 2005, pp. 2141–2146.
23. Head, L., and P. Mirchandani. *RHODES-ITMS*. Report AZ-SP-9701. Arizona Department of Transportation, Phoenix, 1997.
24. Tian, Z., C. Messer, K. Balke, and T. Urbanik. Integration of Diamond Interchange and Ramp Metering Operations. *Transportation Research Record: Journal of the Transportation Research Board*, 2005. 1925: 100–111.
25. Tian, Z. Modeling and Implementation of an Integrated Ramp Metering-Diamond Interchange Control System. *Journal of Transportation Systems Engineering and Information Technology*, Vol. 7, No. 1, 2007, pp. 61–69.
26. Su, D., X. Y. Lu, R. Horowitz, and Z. Wang. Coordinated Ramp Metering and Intersection Signal Control. *International Journal of Transportation Science and Technology*, Vol. 3, No. 2, 2014, pp. 179–192.
27. Achillides, C., and D. Bullock. *Performance Metrics for Freeway Sensor*. FHWA/IN/JTRP-2004/37. Joint Transportation Research Program, Indiana Department of Transportation and Purdue University, West Lafayette, 2004, p. 164.
28. Lu, Y., X. Yang, and G. L. Chang. Algorithm for Detector-Error Screening on Basis of Temporal and Spatial Information. *Transportation Research Record: Journal of the Transportation Research Board*, 2014. 2443: 40–48.
29. Liu, H. X., X. Wu, and P. G. Michalopoulos. Improving Queue Size Estimation for Minnesota's Stratified Zone Metering Strategy. *Transportation Research Record: Journal of the Transportation Research Board*, 2007. 2012: 38–46.
30. Chen, Y. Y., Y. Cheng, and G. L. Chang. Lane Group-Based Traffic Model for Assessing On-Ramp Traffic Impact. *Journal of Transportation Engineering, Part A: Systems*, Vol. 147, No. 2, 2021, p. 04020152.
31. *PTV VISSIM 10 User Manual*. PTV AG: Karlsruhe, Germany, 2018.
32. *Gurobi optimizer reference manual, Version 9*. Gurobi Optimization, LLC., 2020.